Design of Single-Layer Dense Metasurfaces on Irregular Grids Using Discrete Dipole Approximation

Do-Hoon Kwon, *Senior Member, IEEE*

***Abstract*— A design technique for single-layer metasurfaces of planar and conformal profiles utilizing nonperiodic, irregular grids for meta-atom placement is presented. Meta-atoms are placed at the node positions in planar and conformal surface grids created by an unstructured mesher. They are represented by point dipoles using the discrete dipole approximation (DDA), and mutual coupling effects from neighboring resonators are accurately evaluated. Each meta-atom is individualized for representing a desired average current density over the corresponding cell area. Examples of fully reflecting metasurfaces using DDA-based individualized meta-atoms exhibit closer-to-ideal performance than identical meta-atoms on the same grid.**

***Index Terms*— Electromagnetic coupling, electromagnetic reflection, frequency selective surfaces (FSSes), metasurfaces.**

I. Introduction

As a thin-film or surface equivalent of volumetric metamaterials, electromagnetic metasurfaces [1] have demonstrated extraordinary capabilities to transform wave propagation behavior in a thin form factor with low loss. Demonstrated functionalities include anomalous wave reflections and refractions, polarization and angular momentum transformers, leaky-wave antennas, near- and far-field focusing lenses, and holograms [2], [3]. The vast majority of the metasurfaces reported to date are periodic structures, where resonant inclusions are arranged in a periodic lattice on regular square or hexagonal grids. Analysis of a unit cell under periodic boundary conditions (PBCs) with phase shifts permits efficient and accurate prediction of an infinitely periodic structure over a wide range of structural and material complexity in all length scales. In fact, full-wave unit-cell analysis combined with increasing computing powers has been a major enabling force in the development of photonic crystals [4] and electromagnetic bandgap structures [5]. Relaxing the identical cell condition allows local tailoring of transmission and reflection toward overall wavefront manipulation. In an extreme scenario, both meta-atom geometry and their spatial distribution are significantly changed from periodic cases in random metasurfaces [6], [7].

Unit-cell analysis and design have the effect of forcing the grid to be regular and the surface to be planar. Depending on the application, a regular grid in a plane may not be optimal. In planar cases, meta-atoms can be positioned at random locations in random or disordered metasurfaces for enhanced field localization [8] or for modeling realizations using large-scale self-assembly methods [7], [9]. Conformal shapes pose challenges for meta-atom placement. Cylindrical metasurfaces can be rigorously treated using azimuth angle-periodic grids [10], [11]. For singly-curved profiles, individual meta-atoms may be designed using unit-cell analysis assuming an unrolled planar surface environment as an approximation [12]–[14]. However, doubly-curved conformal surfaces are incompatible with unit-cell analysis. Fitting a unit cell on a 3-D conformal surface results in distorting the shapes of the cell and resonator [15].

There are two main challenges in designing doubly-curved conformal 3-D metasurfaces: grid generation for meta-atom placement and mutual coupling effects between meta-atoms. A uniform grid in a 2-D plane can be deformed normal to the grid plane to conform to the desired shape [16], [17]. In these works, the electromagnetic effect of the stretched surface during surface deformation is not addressed. In addition, this surface deformation approach cannot be used to grid an entire closed 3-D surface. For spherical surfaces, frequency selective surfaces (FSSes) in [18]–[20] place resonator elements at equal separations along either one or both of azimuthal and polar angles. The areas occupied by identical elements are not uniform, and the elements can become crowded close to the poles. In [21] and [22], a doubly-curved FSS is approximated as a union of local spherical caps. It is unclear how a two-angle grid on one locally spherical surface for resonator placement can transition into another grid on an overlapping, neighboring spherical surface. As to mutual coupling between elements, a finite array of resonators can be analyzed accurately using full-wave analysis [18], [19], [21]. However, the computational cost becomes prohibitively large as the array size increases. For unit cell-based analysis [17], [20], mutual coupling estimation from periodic analysis is expected to deteriorate in accuracy as the local cell shape and size deviate from those of a reference unit cell. In [23], a surface impedance extraction method for nonuniform and anisotropic conductor patterns

Manuscript received 24 August 2021; revised 11 May 2022; accepted 9 June 2022. Date of publication 24 June 2022; date of current version 17 November 2022. This work was supported by the National Science Foundation under Grant ECCS-1930032.

The author is with the Department of Electrical and Computer Engineering, University of Massachusetts Amherst, Amherst, MA 01003 USA (e-mail: dhkwon@umass.edu).

Color versions of one or more figures in this article are available at https://doi.org/10.1109/TAP.2022.3184537.

Digital Object Identifier 10.1109/TAP.2022.3184537

is reported, where the cell shape is closely related to the impedance anisotropy.

If each meta-atom is approximated by a point dipole, the discrete dipole approximation (DDA) is applicable to metasurface analysis and synthesis. Originally developed to treat interstellar grains [24], the DDA can analyze scattering and absorption by a volumetric body [25]. A body of a continuous medium is discretized into a collection of subvolumes, where each is approximated as a point dipole with an associated polarizability. The response of the entire body is a superposition of individual dipole responses. In metamaterials and metasurfaces, the DDA has been investigated for the analysis and design of surface and volumetric devices for a variety of applications. For effective-medium characterization, homogenization of metamaterials in terms of individual resonator properties has been investigated using the DDA [26]–[28], including bianisotropic media [29], [30]. Dipoles on a lattice structure were analyzed and designed for scattering prediction and control of volumetric devices [31], [32].

For metamaterials comprising an arbitrary or nonperiodic arrangement of resonators, the DDA has been the underlying synthesis principle in many applications. In waveguide environments, polarizabilities of metamaterial elements are modeled [33], [34]. Based on the polarizabilities, cavity-backed metasurface antennas for pattern synthesis are demonstrated [35], extending slotted waveguide antennas with periodic slot elements [36]. For practical finite arrays, the edge or truncation effects can be taken into account [37]. Furthermore, the DDA has been employed to synthesize volumetric holography in the variational limit [38] or in a strong scattering environment [39]. The DDA greatly reduces computational resource requirements for electrically large structures compared with full-wave simulations. While recent advances demonstrate applications to finite device dimensions of practical utility, currently available DDA techniques cannot treat arbitrarily large or infinite structures.

In this article, the DDA is applied to the synthesis of single-layer metasurfaces of planar and doubly-curved profiles of infinite dimensions (or large sizes treated as infinite), comprising a dense array of meta-atoms on irregular grids. Compared with existing DDA-based techniques, infinite structures can be treated by supplementing discrete mutual coupling from neighboring elements with that from an infinite homogenized surface current beyond the neighbors. Starting from a sheet current distribution derived from the desired scattering response, individual meta-atoms are determined from the basic polarizability relation without having to solve matrix equations. Meta-atom size calibration derived from applying the proposed technique to periodic metasurfaces leads to additional performance improvement. Irregular grids for meta-atom placement are provided by an unstructured mesh generator, allowing metasurfaces of doubly-curved as well as planar profiles to be designed, including closed 3-D surfaces. Example planar and conformal metasurface designs for full reflection verify the effectiveness of the design technique. Planar metasurface design in this work is used as a validation for the design technique. The main benefit is for doubly-curved surfaces, which cannot accommodate periodic grids. The proposed technique demonstrates a pathway for metasurfaces based on dense irregular grids toward obtaining performances comparable to those of traditional periodic counterparts, while greatly enhancing the flexibility in surface profile. The approach is limited to a dense array of meta-atoms that can be represented as a continuous sheet impedance and to synthesizing a single scattering response for a given input.

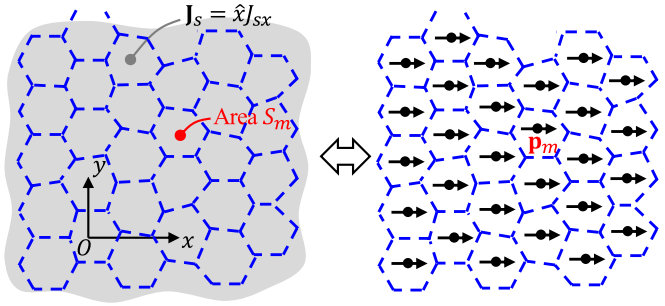

Fig. 1. Spatial averaging or homogenization for a uniform electric surface current density $\mathbf{J}_s = \hat{x}J_{sx}$ in the xy plane as an aperiodic free-space array of point dipoles on an irregular grid. A dipole with a moment $\mathbf{p}_m$ represents a cell area S_m.

In the following time-harmonic treatment, an $e^{j\omega t}$ time convention is assumed and suppressed.

II. Current Homogenization and Irregular Grids

A. Surface Current Homogenization

The ideal response of a passive metasurface to an electromagnetic excitation may be cast in induced surface currents. For wave-transformation applications, the induced currents create scattered fields. The total fields, as desired by the application, are a superposition of incident and scattered fields. Consider a uniform electric surface current density $\mathbf{J}_x = \hat{x}J_{sx}$ in the entire xy plane, shown as the gray shade in Fig. 1. This is appropriate for a single-layer polarizable surface of nonmagnetic constituents, modeled as having zero thickness. For realization of the sheet current using a metasurface, an infinite array of meta-atoms can be arranged in the entire plane. Each meta-atom is responsible for an associated cell, of which the boundary is shown as blue dashed lines.

For *periodic* metasurfaces, the cell boundaries are identical in shape and size. However, each meta-atom may represent a cell of different shape and size, when defined on an irregular grid by design. Let the mth meta-atom represent the homogenized surface current over an area of S_m. Also, we approximate the polarized meta-atom in this cell as a point electric dipole with a dipole moment $\mathbf{p}_m$. For the infinite array of dipoles to be equivalent to the current sheet, we require

$$\mathbf{p}_m = \frac{S_m}{j\omega}\mathbf{J}_s \quad \text{for all } m. \tag{1}$$

The equivalence between the sheet current and the dipole array in Fig. 1 becomes increasingly accurate for smaller cell dimensions.

For a meta-atom having an electric polarizability α, the dipole moment is linearly proportional to the effective E-field

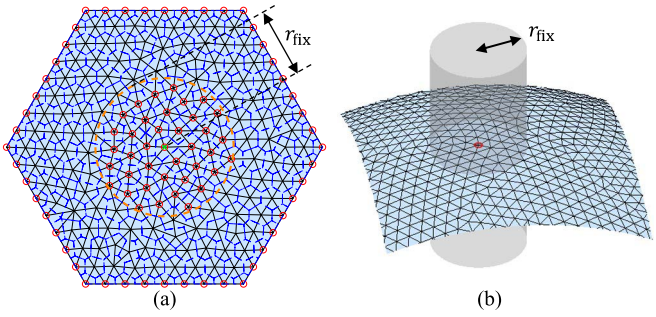

Fig. 2. Examples of planar and curved grids created using an unstructured mesh generator [42]. Nodes of the mesh are the locations for meta-atom placement. (a) Planar grid on a regular hexagon. Red circles indicate fixed node points during mesh generation. The Voronoi diagram defines the cells, bounded by blue dashed lines. This example grid is for designing the meta-atom at the center, marked by a green "×." Nodes within a distance r_{fix} from this meta-atom are used as fixed node points. (b) Portion of a spherical surface grid. For the node indicated by a red circle, a circular cylinder of radius r_{fix} is shown. The cylinder axis passes through the node and is perpendicular to the tangent plane.

that polarizes the dipole [40] or the local excitation E-field, $\mathbf{E}^{\text{loc}}$ [41]. It is the sum of the primary source field and the secondary fields scattered by the entire array except for the dipole under consideration, evaluated at the dipole location. The induced dipole moment $\mathbf{p}$ of the meta-atom is given as

$$\mathbf{p} = \alpha \mathbf{E}^{\text{loc}}. \tag{2}$$

The polarizability α for a given meta-atom is a function of the angular frequency ω, and it is complex-valued even for lossless meta-atoms due to radiation loss by scattering. Knowledge of the needed dipole moment from (1) and the local exciting E-field produces the required value for α, from which the exact shape, size, and material composition of the meta-atom can be determined within a predetermined design space. As a collection of individualized meta-atoms, the metasurface induces the correct equivalent surface current $\mathbf{J}_s$ over the entire surface to generate desired scattered fields upon illumination by the incident wave, realizing the envisioned wave transformation.

B. Irregular Grids Using an Unstructured Mesh Generator

For accommodating flexible node positions especially for conformal surfaces, we take a surface mesh generated by an unstructured mesher as a grid for placing meta-atoms. Specifically, we adopt the 2-D and 3-D mesher by Persson and Strang [42]. For a collection of nodes, a triangular mesh is generated using the Delaunay algorithm [43]. Taking the mesh as a truss structure, the node positions are updated toward force equilibrium over all beams. A converged mesh achieves more-or-less uniform branch lengths between nodes, which are a desirable quality for meta-atom placement in a metasurface.

Irregular grids employed in this article are illustrated in Fig. 2. Fig. 2(a) shows an irregular planar grid on the area of a regular hexagon for designing a meta-atom at the center (marked with a green "×"). Fixed nodes can be specified in a meshing operation, shown as red circular markers. In this example, those along the hexagon boundary are to ensure a smooth transition from this irregular grid to a regular grid in filling an infinite plane, as will be detailed in Section III. A group of nodes within a distance r_{fix} from the meta-atom under design are chosen as fixed nodes during meshing. These fixed grid points are used for accurate near-neighbor coupling evaluation in a conformal metasurface design, as will be described in Section V. Nodes in the intervening region (those without red circle markers) are filled in by the mesher. Visually, there are no extremely short or long branches. The specification of the mesh is given as a Delaunay triangulation of the nodes. Meta-atoms are to be positioned at the node locations. The cell occupied by one meta-atom is given by the associated Voronoi cell [43]. Cell boundaries are indicated by blue dashed lines in Fig. 2(a).

An example mesh on a doubly-curved surface is shown in Fig. 2(b).[1] While those having six branches are most common, nodes connected to five or seven branches are also observed. As meta-atoms are placed at the node locations, no extremely short or long branches indicate that the local density of meta-atoms will be more-or-less uniform on this conformal grid. Furthermore, this grid generation approach is applicable to metasurfaces in the form of whole closed surfaces. For the node indicated by a red circle, an imaginary circular cylinder of radius r_{fix} is formed to determine the near-neighbor nodes illustrated in Fig. 2(a). In Section V, coupling from meta-atoms at these near-neighbor nodes is evaluated taking into account their positions. The process of finding near-neighbor nodes is repeated for each meta-atom in the metasurface.

III. Planar Metasurfaces

To develop and validate the design technique for metasurfaces on planar irregular grids, we adopt a grid structure in Fig. 3(a). The circle markers indicate meta-atom positions. A regular hexagonal grid with an interelement distance of p_0 serves as the reference periodic grid for performance assessment. In the xy plane, a regular hexagon of a side s_0 is centered at the coordinate origin, referred to as a supercell. An irregular grid is formed on the supercell, where red circles indicate the node positions. Nodes on the supercell boundary are fixed during the meshing operation to coincide with regular grid points, as illustrated in Fig. 2(a). The irregular grid transitions to a periodic hexagonal grid with a cell size of p_0 beyond the supercell boundary, extending to infinity. The periodic nodes are indicated by blue circles. The example grid in Fig. 3(a) uses $p_0 = 0.32\lambda$ (λ = free-space wavelength) and $s_0 = 5p_0$. In this work, the cell size of $p_0 = 0.32\lambda$ is chosen based on the radiansphere dimension (a radius of $\lambda/2\pi \approx 0.159\lambda$) of a small dipole antenna, which represents the size of its near-field region [44]. Other subwavelength reference cell dimensions are certainly possible.

[1]The mesher in [42] does not mesh a curved surface natively. Hence, a volume that has the desired curved surface as its bounding surface can be first meshed. Then, nodes on the bounding surface and the connectivity among them can be extracted.

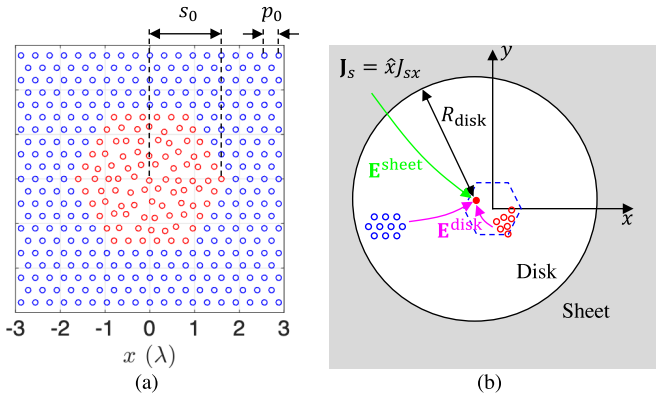

Fig. 3. Meta-atom design on a planar irregular grid. (a) Example overall grid for meta-atom positions in the xy plane. The supercell containing an irregular grid (red circles) is surrounded by regular hexagonal grid points (blue circles) extending to infinity. The grid in Fig. 2(a) is another example of a supercell. The period of cell placement on the regular grid is p_0. The side of the large hexagonal supercell is s_0. (b) Partition of the infinite grid into regions of discrete and continuous contributions for the local E-field evaluation at a meta-atom of interest (a solid red circle).

For a plane-wave illumination at normal incidence, it is desired that meta-atoms on the grid in Fig. 3(a) present a *uniform* homogenized electric surface current density $\mathbf{J}_s$. Then, individual dipole moments are quantitatively determined from (1). If there are N meta-atoms on the supercell, the cell area S_n $(n = 1, \ldots, N)$ is found from the associated Voronoi cell definition. The cell area for the reference dipole moment $\mathbf{p}_{\text{ref}}$ is $S_{\text{ref}} = (\sqrt{3}/2)p_0^2$.

At the location $\mathbf{r}_m$ of the mth meta-atom, the local E-field $\mathbf{E}_m^{\text{loc}}$ is a sum of the external and interaction fields, i.e.,

$$\mathbf{E}_m^{\text{loc}} = \mathbf{E}_m^{\text{ext}} + \mathbf{E}_m^{\text{int}}. \tag{3}$$

The external field, $\mathbf{E}_m^{\text{ext}}$, is the field due to the primary source, which is that of the incident plane wave. The interaction field, $\mathbf{E}_m^{\text{int}}$, is the sum of the E-field contributions from all other dipoles observed at $\mathbf{r}_m$. It is evaluated using the DDA with a distinction from conventional periodic cases [40], [41] in that meta-atoms are not positioned on a strictly periodic grid. In addition, a numerically efficient calculation is performed for $\mathbf{E}_m^{\text{int}}$ by partitioning the entire metasurface into discrete and continuous polarization regions [41], [45] using a circle of radius R_{disk} centered at $\mathbf{r}_m$. For the dipole at $\mathbf{r}_m$ indicated as a solid red circle, this partition of the xy plane is illustrated in Fig. 3(b). The interaction field is a sum of discrete dipole contributions from inside the circular disk and a continuous sheet current distribution from outside the disk

$$\mathbf{E}_m^{\text{int}} = \mathbf{E}_m^{\text{sheet}} + \mathbf{E}_m^{\text{disk}}. \tag{4}$$

A smaller radius R_{disk} (i.e., fewer discrete dipole contributions) is needed to find convergence for $\mathbf{E}_m^{\text{int}}$ with an increasing element density [41]. To ensure numerical convergence, $R_{\text{disk}} = 500p_0$ is used for all interaction field computations in this article.

For a homogeneous $\mathbf{J}_s$ that is tangent to the metasurface, the sheet current contribution is analytically given by [41]

$$\mathbf{E}_m^{\text{sheet}} = -\mathbf{J}_s \frac{\eta}{4}\left(1 - \frac{1}{jkR_{\text{disk}}}\right)e^{-jkR_{\text{disk}}} \tag{5}$$

where $k = 2\pi/\lambda$ is the free-space wavenumber and $\eta \approx 377\ \Omega$ is the free-space intrinsic impedance. The interaction field contribution from within the disk is a discrete sum

$$\mathbf{E}_m^{\text{disk}} = \sum_{\substack{n \neq m \\ R_{mn} < R_{\text{disk}}}} \mathbf{E}_{mn} \tag{6}$$

over the E-field $\mathbf{E}_{mn}$ due to the nth dipole at $\mathbf{r}_n$ observed at $\mathbf{r}_m$, where $R_{mn} = |\mathbf{R}_{mn}|$ and $\mathbf{R}_{mn} = \mathbf{r}_m - \mathbf{r}_n$. The point dipole field $\mathbf{E}_{mn}$ is expressed as [41], [46]

$$\mathbf{E}_{mn} = \frac{1}{4\pi\epsilon_0}\left\{k^2(\hat{R} \times \mathbf{p}_n) \times \hat{R}\frac{e^{-jkR_{mn}}}{R_{mn}} + [3\hat{R}(\hat{R} \cdot \mathbf{p}_n) - \mathbf{p}_n]\left(\frac{1}{R_{mn}^3} + \frac{jk}{R_{mn}^2}\right)e^{-jkR_{mn}}\right\}. \tag{7}$$

In (7), $\epsilon_0 \approx 8.854 \times 10^{-12}$ F/m is the free-space permittivity and $\hat{R} = \mathbf{R}_{mn}/R_{mn}$.

Let us denote the meta-atom size by the radius a of the smallest circumscribing sphere [see Fig. 4(a)]. We note that α_{DDA} inverted from (2) is a complex-valued quantity that needs to be mapped to a real-valued dimension a_{DDA}. For this purpose, the plane-wave reflection phase is chosen as the intermediate real-valued function of α_{DDA}. For a meta-atom at $\mathbf{r}_m$ with an extracted polarizability α_{DDA} occupying a cell area of S_m, let us denote the interaction field for a uniform, unit surface current of 1 A/m amplitude by $\mathbf{e}_m^{\text{int}}$ [having a unit of (V/m)/(A/m) = Ω]. Then, the plane-wave reflection coefficient Γ_{DDA} associated with this polarizability can be shown to be

$$\Gamma_{\text{DDA}} = -\frac{\eta}{2}\frac{(j\omega\alpha_{\text{DDA}}/S_m)}{1 - (j\omega\alpha_{\text{DDA}}/S_m)\hat{x} \cdot \mathbf{e}_m^{\text{int}}}. \tag{8}$$

The one-to-one correspondence between the reflection phase and the meta-atom size is used to translate α_{DDA} to a_{DDA} via $\angle\Gamma_{\text{DDA}}$.

In summary, designing a planar metasurface on an irregular grid amounts to finding individualized meta-atom dimensions that collectively induce the required the uniform surface current associated with a desired transmission and reflection property. An unstructured mesher provides an irregular grid for a nominal or average cell size p_0 for meta-atom placement. Then, individual meta-atom design follows this process:

1) Partition the entire metasurface into two regions using a circular disk of radius R_{disk} centered at the meta-atom location $\mathbf{r}_m$.
2) Evaluate $\mathbf{E}_m^{\text{loc}}$ using (5) and (6) for $\mathbf{E}_m^{\text{int}}$.
3) Invert (2) to find the required polarizability α_{DDA}.
4) Use (8) to find the meta-atom size associated with α_{DDA}.
5) Perform meta-atom size calibration using the process in Section IV.

The final calibration provides a minor correction to the retrieved meta-atom dimension based on (2). For this purpose, a periodic metasurface with a cell size p_0 needs to be designed and analyzed for the same functionality.

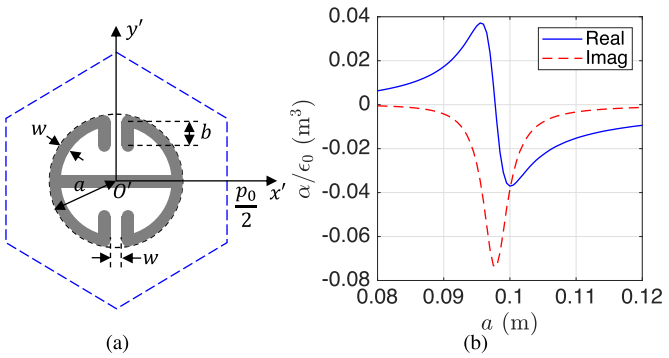

Fig. 4. Planar PEC dipole and its polarizability. (a) End-loaded planar dipole in the $x'y'$ plane contained in a circle of radius a. The gray shade indicates the conductor pattern. The regular hexagon in dashed blue indicates the PBC boundary when the dipole is placed on a periodic grid as an array element. (b) Polarizability along the x-axis direction with respect to a at 300 MHz for $w = a/5$ and $b = 0.0738a$.

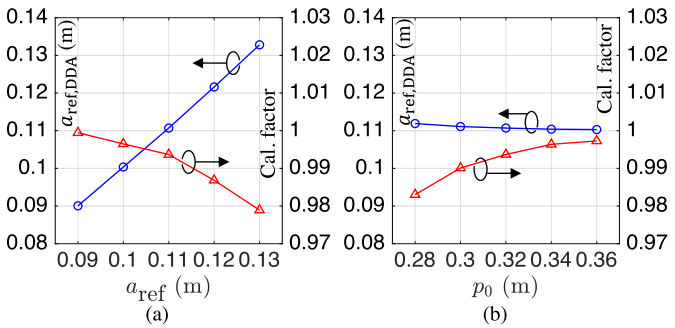

Fig. 5. Calibration characteristics with respect to meta-atom and cell dimensions. The DDA-derived dipole dimension and the calibration factor for (a) fixed cell size at $p_0 = 0.32$ m with respect to a_{ref} and (b) fixed meta-atom size at $a_{\text{ref}} = 0.11$ m with respect to p_0.

IV. Meta-Atom Size Calibration

For each dipole $\mathbf{p}_m$ on the irregular grid, (2) can be inverted for the required polarizability, α_m, using (1) and (3). In relating the retrieved polarizability to an individualized meta-atom via (8), the fact that a small physical meta-atom behaves *approximately* as a point dipole leads to less-than-ideal performance for an irregular-grid metasurface designed using the proposed DDA-based approach compared with a periodic counterpart designed using the unit-cell technique. A first-order correction can be applied to improve the DDA-based meta-atom design using a "calibration" process on a reference periodic metasurface. The rationale is that the proposed technique should produce the same design as the unit-cell technique when applicable—for periodic metasurfaces.

Let us illustrate this calibration correction with a periodic single metallic-layer metasurface for full reflection. Made out of perfect electric conductor (PEC), a planar end-loaded dipole in the $x'y'$ plane contained in a circle of radius a is shown in Fig. 4(a). It is centered at the coordinate origin O' and the dipole axis is along the x'-axis. The width b of the parallel section helps control the resonant frequency without changing the dipole size. At a frequency of $f = 300$ MHz ($\lambda = 1$ m), the polarizability with respect to a is plotted in Fig. 4(b) for $w = a/5$ and $b = 0.0738a$. It has been numerically obtained using Altair FEKO as described in the Appendix. Here, a particular choice of $b = 0.0738a$ has been made such that when the $a = a_{\text{ref}} = 0.1$ m dipole is placed in a periodic hexagonal grid with $p_0 = 0.32$ m [see the cell boundary in Fig. 4(a)], the resulting metasurface fully reflects an $\hat{x}$-polarized incident plane wave at normal incidence. For this reference periodic metasurface, the polarizability is extracted from (2) and mapped to a dipole dimension $a_{\text{ref, DDA}} = 0.100352$ m, which is slightly different from a_{ref}. Hence, a dimension scaling by a factor $a_{\text{ref}}/a_{\text{ref, DDA}}$ is applied as a calibration to all DDA-derived dipole dimensions.

To understand the calibration characteristics, numerical experiments are performed. For a periodic structure with a fixed cell size $p_0 = 0.32$ m, a few different metasurfaces using a dipole meta-atom in Fig. 4(a) with size $a = a_{\text{ref}} \in [0.09, 0.13]$ m are designed. For each size a_{ref}, the length b is adjusted to make the dipole array resonant at 300 MHz. The retrieved dipole size $a_{\text{ref,DDA}}$ and the associated scale factor are plotted in Fig. 5(a). The DDA approach tends to predict $a_{\text{ref,DDA}} > a_{\text{ref}}$, with the amount of overestimation increasing with a_{ref}. Nearly no calibration is needed at the small dipole with $a_{\text{ref}} = 0.09$ m, but a 2% correction is needed at $a_{\text{ref}} = 0.13$ m. This agrees with the understanding that the dipole-mode scattering becomes increasingly dominant with a decreasing size. Next, fully-reflecting periodic metasurfaces are designed for a fixed dipole size $a_{\text{ref}} = 0.11$ m, while the cell size is varied in $p_0 \in [0.28, 0.36]$ m. The retrieved meta-atom size and the calibration factor are plotted in Fig. 5(b). A smaller meta-atom size correction is needed with a larger element spacing. Again, this is consistent with the fact that a dipole scattering term becomes dominant when observed farther away from a small, physical meta-atom.

In individualizing meta-atom dimensions in this design technique, the DDA-based polarizability information is the main deciding factor. Size calibration is expected to provide a minor correction of varying degrees, depending on the meta-atom size and element spacing.

V. Doubly-Curved Conformal Metasurfaces

For doubly-curved conformal surfaces, we limit our attention to smooth curved surfaces with a large radius of curvature. At a meta-atom location, the surface is assumed to be locally planar, as is often adopted in conformal metasurface or FSS designs [13], [15], [17], [20], [47]–[49]. The interaction field at a meta-atom is evaluated following Section III in the local plane. This approximation is needed for large or infinite metasurfaces for which discrete interaction field evaluation using the DDA approach alone is not practical. The distinction is that meta-atom positions in the local plane are at non-periodic locations defined by the mesher-generated irregular grid.

The interaction field at a meta-atom location will be most significantly impacted by the near-neighbor elements. For a given meta-atom at $\mathbf{r}_m$, a cylinder of radius r_{fix} in Fig. 2(b) determines these near-neighbor elements that are incorporated in the evaluation of $\mathbf{E}_m^{\text{int}}$ as fixed grid points. These neighboring elements are then projected onto the tangent plane at $\mathbf{r}_m$. This is illustrated in Fig. 6(a) using a parabolic surface example,

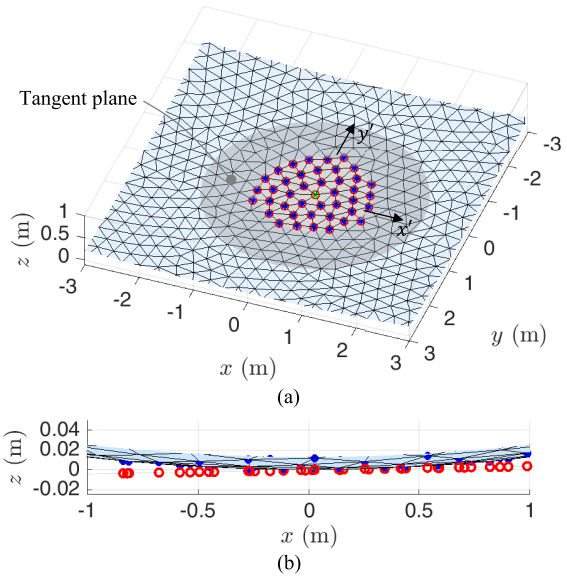

Fig. 6. Doubly-curved grid and the local planarity approximation for conformal metasurface design. The example surface is a paraboloid with a focal length $F = 20$ m and a vertex at the coordinate origin. (a) Projection of a group of nodes onto a tangent plane. The node under design is marked by a green "×" at the local coordinate origin $(x', y') = (0, 0)$. Blue asterisks are conformal nodes inside the cylinder of radius $r_{\text{fix}} = 3.5p_0$ in Fig. 2(b). Red circles are their projections onto the tangent plane. (b) View from the $-y$-axis direction. The z-axis scale has been expanded for clarity.

where a paraboloid with a focal length $F = 20$ m and the vertex at the coordinate origin is meshed using a nominal branch length (the interelement spacing) of $p_0 = 0.32$ m. The meta-atom location of interest is marked by a green "×" near the origin. Blue asterisks indicate a total of 41 neighboring nodes that fall inside a cylinder with $r_{\text{fix}} = 3.5p_0$. A plane at $\mathbf{r}_m$ tangent to the curved surface is shown as a gray translucent disk, defining a local $x'y'$ plane with its origin O' at $\mathbf{r}_m$. The 41 nodes are then projected onto this tangent plane, shown as red circles. A side view of the configuration is shown in Fig. 6(b). This conformal surface mesh will be used to design a metasurface parabolic reflector in Section VI-B at $f = 300$ MHz. Since the smallest radius of curvature of a parabolic surface is equal to $2F$ at the vertex, the longest possible projection distance is $r_{\text{fix}}^2/4F$. For the given example, it is a small fraction of the wavelength at 0.016λ.

Next, in the tangent plane, a planar metasurface is constructed and analyzed following the procedure in Section III, using the projected group of nodes as fixed points during 2-D mesh generation. In fact, Fig. 2(a) is the planar grid in a regular hexagonal supercell in the $x'y'$ plane for the node under consideration in Fig. 6 using $s_0 = 8p_0$. The supercell is augmented by an array of regular grid points to form an infinite planar array, as illustrated in Fig. 3(a). The local E-field for the meta-atom under design is efficiently evaluated by partitioning the plane into continuous and discrete current contribution regions [see Fig. 3(b)]. The required polarizability α_{DDA} is found from (2) and the associated meta-atom dimension a_{DDA} retrieved using $\angle\Gamma_{\text{DDA}}$ in (8). Since $\mathbf{E}_m^{\text{sheet}}$ in (5) assumes a planar surface, evaluation of $\mathbf{E}_m^{\text{int}}$ via (4) becomes inaccurate for curved surfaces. Nevertheless, it is expected to be approximately valid and not a concern for a large radius of curvature. This is confirmed with a curved metasurface design in Section VI-B.

Since the group of near neighbors are different from element to element on an irregular grid on a conformal surface, this design procedure should be repeated for each meta-atom. Hence, the metasurface design time linearly scales with the total number of meta-atoms.

In summary, a doubly-curved metasurface is a collection of individualized meta-atoms at irregular node locations of an unstructured surface mesh. For meta-atom placement, a conformal mesh with a nominal branch length p_0 is generated. Separately, for the purpose of size calibration, a planar, periodic metasurface on a hexagonal grid with a period p_0 is generated and analyzed. The meta-atom dimensions are compared between the unit-cell and DDA methods to find the calibration scale factor $a_{\text{ref}}/a_{\text{ref, DDA}}$. Then, the process for designing a meta-atom at $\mathbf{r}_m$ is as follows:

1) Find the neighboring meta-atoms that will be incorporated as fixed nearby points in the local E-field evaluation. For this purpose, a cylinder of radius r_{fix} with its axis passing through $\mathbf{r}_m$ can be used.
2) Project the neighboring elements onto the tangent plane at $\mathbf{r}_m$.
3) Form a regular hexagonal supercell with a side length s_0 using the projected neighboring nodes as fixed grid points.
4) Augment the supercell with periodic nodes with a period p_0 to fill the entire tangent plane.
5) Partition the tangent plane into two regions using a circular disk of radius R_{disk} centered at $\mathbf{r}_m$.
6) Evaluate $\mathbf{E}_m^{\text{loc}}$ using (5) and (6) for the $\mathbf{E}_m^{\text{int}}$ portion.
7) Invert (2) to find the required polarizability α_{DDA}.
8) Use (8) to find the meta-atom size a_{DDA} at $\mathbf{r}_m$. Perform size calibration using a scale factor $a_{\text{ref}}/a_{\text{ref, DDA}}$.

This process should be performed for every meta-atom on the metasurface.

VI. Numerical Examples

Example metasurface designs are presented for full reflection without transmission. They serve a good validation purpose because zero overall transmission is possible only when local transmission does not occur anywhere.

A. Fully-Reflecting Planar Metasurface/FSS

For planar metasurfaces, unit cell-based designs are well established with good performance. Here, we test a planar metasurface design on an irregular grid for validation before treating a doubly-curved surface toward practical applications that can benefit from irregular grids. The design process summarized at the end of Section III is followed.

Consider a planar metasurface in the xy plane comprising a free-standing array of planar dipoles in Fig. 4(a). At $f = 300$ MHz, an $\hat{x}$-polarized unit plane wave with the incident E-field $\mathbf{E}^{\text{i}} = \hat{x}e^{-jkz}$ V/m illuminates the metasurface at normal incidence. Full copolarized reflection, i.e., without

cross-polarized transmission or reflection, is desired. For an incident plane wave, a passive and lossless uniform metasurface can be treated as a two-port network described by the reflection and transmission coefficients, Γ and τ, defined as the ratio of the reflected and transmitted tangential E-field amplitudes to that of the incident wave at the surface, respectively. A single-layer metasurface that supports an electric surface current maintains continuity of the tangential E-field across the metasurface. Then, the magnitude and phase of Γ are related by

$$\angle\Gamma = \cos^{-1}(-|\Gamma|). \tag{9}$$

The homogenized surface current associated with Γ is

$$J_{sx} = -\frac{2}{\eta}\Gamma \tag{10}$$

for the given incident wave. Hence, either $|\Gamma|$ or $\angle\Gamma$ determines the required surface current density to achieve a particular response. Full copolarized reflection requires $\mathbf{J}_s = \hat{x}(2/\eta) \approx \hat{x}5.31$ mA/m.

Based on a reference periodic hexagonal grid with $p_0 = 0.32$ m, a supercell of irregular grid points is formed using $s_0 = 5p_0$. The grid points are obtained by perturbing the reference, regular grid points. In terms of a pair of indices (i, ℓ), the reference periodic nodes are located at

$$(x_{i\ell}, y_{i\ell}) = \left((i-1)p_0 + (\ell-1)\frac{p_0}{2}, (\ell-1)\frac{\sqrt{3}p_0}{2}\right). \tag{11}$$

Each internal node (excluding those on the supercell perimeter) is shifted to

$$x_{i\ell} \to x_{i\ell} + \Delta\rho\cos\Phi, \quad y_{i\ell} \to y_{i\ell} + \Delta\rho\sin\Phi \tag{12}$$

where $\Delta\rho \sim U[\Delta\rho_{\max}/2, \Delta\rho_{\max}]$ and $\Phi \sim U[0, 2\pi]$ are random variables following uniform distributions. The maximum perturbation in distance is set to $\Delta\rho_{\max} = 0.22p_0$. One random supercell realization is shown in Fig. 3(a) and it is used in this reflector example.

There are a total of 91 nodes in the supercell, which can be addressed using a compound index m ($m = 1, \ldots, 91$) instead of (i, ℓ) for brevity. For all supercell nodes, magnitude distributions of the E-field components are plotted in Fig. 7(a). The external E-field, $\mathbf{E}_m^{\text{ext}}$, has a magnitude of unity for all nodes, associated with the incident unit plane wave. Obtained using $R = 500p_0$, the sheet contribution has $|\mathbf{E}_m^{\text{sheet}}| = 0.50$ V/m for all nodes. The circular disk contribution, $\mathbf{E}_m^{\text{disk}}$, changes from node to node. As a result, the local E-field, $\mathbf{E}_m^{\text{loc}}$ is different for each node, with the magnitude ranging from 0.304 to 0.842 V/m. In comparison, the unperturbed regular grid produces $|\mathbf{E}_m^{\text{disk}}| = 0.440$ V/m and $|\mathbf{E}_m^{\text{loc}}| = 0.561$ V/m, uniform across all nodes. The dipole dimensions retrieved using (2) and (8) are plotted in Fig. 7(b). The dipole radius varies from node to node, around the reference size of $a_{\text{ref}} = 0.1$ m. The largest and smallest radii are 0.1022 and 0.0971 m, respectively.

After the DDA-derived meta-atoms are calibrated in size, the resulting metasurface design is numerically tested for the transmission and reflection responses. The overall grid the metasurface is designed upon is infinite and nonperiodic owing to the irregular grid points in the supercell. We note that the meta-atoms in the supercell are designed to present a homogenized current $\mathbf{J}_s$ on the individual cell level. To use a commercially available tool to assess the performance, PBCs are applied to the supercell boundary,[2] effectively making the metasurface a periodic structure on a regular hexagonal grid with a center-to-center distance between neighboring supercells of $\sqrt{3}s_0 = 5\sqrt{3}p_0 = 2.771$ m. The supercell is modeled in FEKO and analyzed under unit plane-wave illumination. As shown in Fig. 8(a), the supercell shape needs to be modified to a parallelogram before PBCs can be applied in FEKO. The induced current magnitude is different for different meta-atoms, as expected.

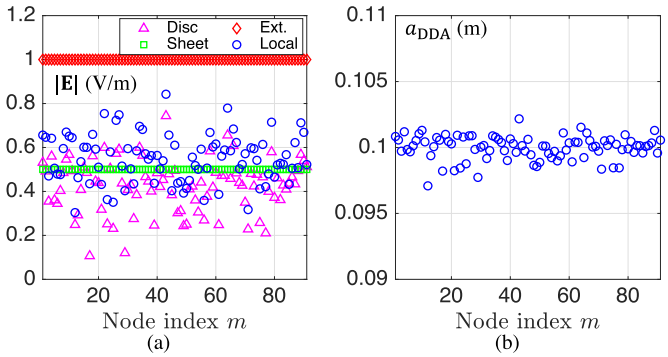

Fig. 7. Meta-atom design for a metasurface reflector on an irregular grid at 300 MHz. The hexagonal supercell with $s_0 = 5p_0$ and $p_0 = 0.32$ m has 91 nodes. (a) E-field magnitudes—$|\mathbf{E}^{\text{disk}}|$, $|\mathbf{E}^{\text{sheet}}|$, $|\mathbf{E}^{\text{ext}}|$, and $|\mathbf{E}^{\text{loc}}|$—in V/m for unit plane-wave illumination at normal incidence at different node positions. (b) Dipole size a_{DDA} retrieved from the DDA-based meta-atom design process.

For this supercell under PBCs at 300 MHz, there are 19 propagating Floquet modes. These propagating modes can be addressed using a single compound index q. In the top-left inset in Fig. 8(b), the mode index q is indicated next to the propagation direction in the $(u, v) = (\sin\theta\cos\phi, \sin\theta\sin\phi)$ plane in terms of the standard spherical (r, θ, ϕ) coordinates. The fundamental Floquet mode associated with normal incidence, $(u, v) = (0, 0)$, is $q = 10$. Fig. 8(b) compares the transmission and reflection of four metasurfaces: the "reference" design based on a unit cell of size p_0 (red markers), the "baseline" metasurface on the same irregular grid with all meta-atom sizes fixed at $a = a_{\text{ref}}$ (i.e., not individualized; green markers), the "uncalibrated" DDA-based metasurface with individualized meta-atom dimensions without size calibration (cyan markers) and, the "calibrated" DDA-based metasurface (blue markers). The reflection and transmission coefficients for the (0, 0)-order Floquet mode are summarized in Table I for the four metasurfaces. The reference design has nominally perfect reflection. If the meta-atom size is unchanged while being placed on the irregular grid, the resulting baseline metasurface

[2]When the supercell in Fig. 3(a) is placed under PBCs, cells along a pair of opposite sides fall at identical locations. There are three such pairs of sides. Also, three supercell corner points end up at the same location. There are two sets for corners. Hence, elements along the sides and corners in periodic simulations in FEKO are taken to have the average radii of the relevant DDA-based meta-atoms.

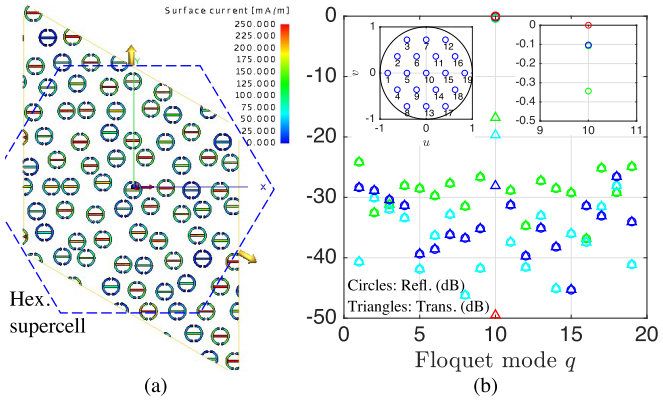

Fig. 8. Scattering characteristics of the DDA-based planar metasurface reflector on an irregular grid at 300 MHz. (a) Magnitude distribution for the induced surface current on the dipole elements. (b) Reflection and transmission in fractional power for all propagating Floquet modes. Red markers are associated with the reference reflector based on unit-cell analysis. Green markers are for the baseline case on the irregular grid, where all dipole dimensions are fixed at $a = a_{\text{ref}} = 0.1$ m. Blue and cyan markers represent the performance of the DDA-based designs with and without calibration, respectively.

TABLE I

COMPARISON OF REFLECTION AND TRANSMISSION IN THE FUNDAMENTAL (0, 0) FLOQUET MODE

Design	Reference	Baseline	Uncalibrated	Calibrated
$\|\Gamma\|$ (dB)	-2.98×10^{-5}	−0.344	−0.108	−0.103
$\|\tau\|$ (dB)	−49.5	−16.81	−19.68	−28.09

characteristics deteriorate. Even without size calibration, the DDA-derived metasurface significantly improves reflection and transmission toward the ideal characteristics. Meta-atom size calibration further improves the performance. Cross-polarized reflection and transmission are low at −55.08 dB. Transmission and reflection in undesired propagating Floquet modes ($q \neq 10$) are also shown in Fig. 8(b) for the baseline, and DDA-derived metasurfaces with and without calibration. Each marker indicates the sum of fractional powers for copolarized and cross-polarized reflected or transmitted waves. It is clear that the DDA-derived metasurface lowers the amount of power diverted into undesired propagating modes.

Unlike the reference design comprising identical unit cells, individualized meta-atoms of the DDA-based design will have different frequency dispersion between elements. Hence, it is of interest to inspect the reflector performance with respect to frequency. For the fundamental Floquet mode, the reflection and transmission coefficient magnitudes are compared in Fig. 9 between the reference, baseline, and DDA-based metasurfaces before and after calibration from 280 to 320 MHz. It is observed that the DDA-based reflector performance approaches that of the reference reflector over the bandwidth compared with the baseline design, where the meta-atoms are not individualized. Collectively, the uncalibrated design has a resonant frequency slightly shifted down from 300 MHz. The meta-atom size calibration assists in restoring the resonant frequency to the design frequency. For the DDA-based reflector,

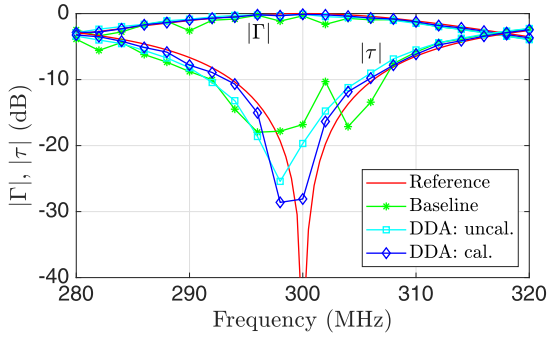

Fig. 9. Comparison of the reflection and transmission coefficients for the fundamental Floquet mode ($q = 10$) with respect to frequency between the reference, baseline, and DDA-based planar metasurface reflectors.

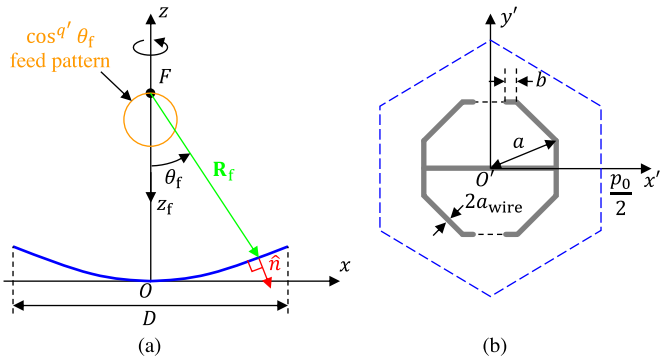

Fig. 10. Parabolic reflector design as a curved metasurface. (a) xz plane cut of a parabolic reflector configuration with a diameter D and a focal length F. The configuration is rotationally symmetric with respect to the z-axis. (b) End-loaded PEC thin-wire dipole meta-atom with a wire radius a_{wire} in the $x'y'$ plane. The axis of the loading wire follows a regular octagonal contour contained in a circle of radius a. The regular hexagon in dashed blue indicates the PBC boundary for periodic analysis of the reference metasurface.

fractional powers converted into higher-order Floquet modes remain low.

B. Parabolic Metasurface Reflector Antenna

As an example employing a doubly-curved metasurface for full reflection, consider a prime-focus parabolic reflector antenna with a reflector diameter D and a focal length F. It is desired that the parabolic reflector be designed as a metasurface comprising a free-standing array of dipole meta-atoms in place of a solid conductor reflector at a design frequency. While a free-standing dipole array is not practical, it serves as a validation case for conformal metasurface design on an unstructured grid. The design process summarized at the end of Section V is followed.

The configuration is shown in Fig. 10(a). The feed is modeled using a far-field pattern with the phase center at the focal point, giving the feed E-field at a point (x, y, z) as

$$\mathbf{E}_f = \hat{e}_f \frac{e^{-jkR_f}}{R_f} \cos^{q'}\theta_f, \quad 0 \leq \theta_f < \frac{\pi}{2} \tag{13}$$

where $R_f = |\mathbf{R}_f|$ and $\mathbf{R}_f = \hat{x}x + \hat{y}y + \hat{z}(z - F)$. In (13), the angle θ_f measures from the z_f-axis, which is equal to the $-z$-axis. The feed pattern is zero in $\pi/2 < \theta_f \leq \pi$, which

corresponds to $0 \leq \theta < \pi/2$. The polarization unit vector is given by

$$\hat{e}_{\rm f} = \frac{\hat{R}_{\rm f} \times \hat{R}_{\rm f} \times \hat{x}}{|\hat{R}_{\rm f} \times \hat{R}_{\rm f} \times \hat{x}|}, \quad \hat{R}_{\rm f} = \frac{\mathbf{R}_{\rm f}}{R_{\rm f}}. \tag{14}$$

This represents an x-directed electric current source with an ideal rotationally symmetric pattern, given as a cosine raised to a q'th power [50].

Let us consider a reflector with $D = F = 20$ m at $f = 300$ MHz. The parabolic surface is meshed with a nominal branch length $p_0 = 0.32$ m. To take advantage of the numerically efficient thin-wire method of moments formulation, we choose a thin-wire dipole shown in Fig. 10(b) as the meta-atom instead of a planar dipole. A PEC wire of radius $a_{\rm wire}$ is used for its construction. The end-load wire axis traces a regular octagonal perimeter contained in a circle of radius a in the $x'y'$ plane, centered at O'. The reference metasurface on a periodic hexagonal grid with $p_0 = 0.32$ m is first analyzed to find $a = a_{\rm ref} = 0.1$ m, $b = 0.0877a$, and $a_{\rm wire} = 1$ mm for full reflection at normal incidence. For the reference metasurface, the DDA process produces $a_{\rm ref,\,DDA} = 0.100443$ m. Hence, the geometrical scaling factor for calibration is determined to be $a_{\rm ref}/a_{\rm ref,\,DDA} = 0.1/0.100443$.

The curved mesh for the 20 m diameter reflector contains 3641 nodes for meta-atom placement. For each meta-atom, near-neighbor elements within a cylinder of $r_{\rm fix} = 3.5p_0$ are incorporated as fixed grid points in generating a regular hexagonal supercell with $s_0 = 8p_0$. For the element closest to the paraboloid vertex at the coordinate origin O, the near-neighbor selection and projection to the tangent plane are shown in Fig. 6. The resulting supercell in the tangent plane is in Fig. 2(a). For meta-atoms near the boundary of the reflector surface, the truncation effect is not considered in their design. During surface meshing, a parabolic surface that extends beyond the reflector boundary is meshed such that near-neighbor elements within the distance $r_{\rm fix}$ are available for every meta-atom on the reflector for applying the DDA procedure. The DDA-derived dipole dimensions $a_{\rm DDA}$ for the 3641 elements range from 0.09805 to 0.10161 m, with an average value of 0.10056 m. While evaluation of $\mathbf{E}_m^{\rm sheet}$ from a homogenized infinite sheet current allows treatment of infinite metasurfaces, the downside is that truncation effects cannot be incorporated for elements near structural boundaries. For finite metasurfaces, standard DDA-based methods exist for incorporating edge effects [37].

After the meta-atom dimensions are calibrated, the dipole elements are modeled in FEKO. The feed pattern is determined such that the pattern diminishes by 10 dB at the reflector rim compared with the reflector center. It is found that $q' = 9.20$. The metasurface reflector excited by the pattern-defined feed is analyzed using FEKO for the induced wire current (involving 120 058 method-of-moments unknowns) and the result is shown in Fig. 11. As anticipated, a position-dependent dipole current distribution is obtained. A detailed view of the dipole geometry and the induced current near O is shown in the inset. For a dipole at position $\mathbf{r}_m$ in the Cartesian (x, y, z) system, a local (x', y', z') coordinate system is defined with its origin O' at $\mathbf{r}_m$. The axis and plane of the dipole are set to satisfy

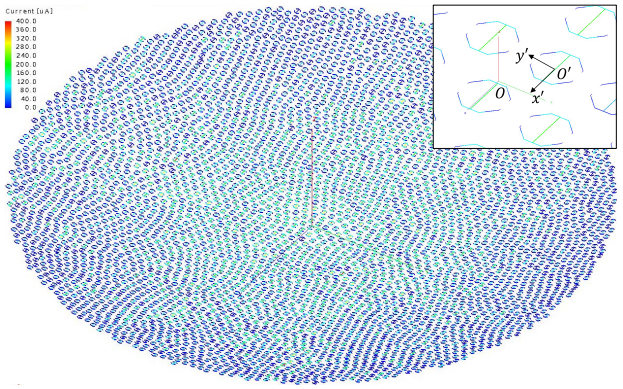

Fig. 11. Induced wire current magnitude distribution on the meta-atoms comprising the parabolic metasurface reflector of a 20λ diameter and a 20λ focal length. The metasurface reflector comprises 3641 dipole meta-atoms. The inset shows a magnified view near the paraboloid vertex at O.

$$\hat{x}' \parallel \hat{e}_{\rm f} - \hat{n}(\hat{n} \cdot \hat{e}_{\rm f}) \text{ and } \hat{z}' = \hat{n} \tag{15}$$

where $\hat{n}$ is the unit surface normal at $\mathbf{r}_m$, as illustrated in Fig. 10(a). In other words, the orientation of a meta-atom is determined such that the dipole axis is aligned with the feed E-field projected onto the reflector surface and the dipole is in the tangent plane at $\mathbf{r}_m$.

The pattern characteristics of the metasurface reflector antenna are compared with those of the reference antenna that uses a solid PEC reflector. At the design frequency, the directivity $D(\theta, \phi)$ of the metasurface reflector antenna is compared in Fig. 12(a) with that of the reference antenna in the E-plane. For the copolarized component, the metasurface reproduces the main beam and a few sidelobes of the reference pattern accurately. Farther away from the main beam, the overall angular trend remain similar between the two antennas. The maximum directivity is 35.08 dBi, correctly realized in the $+z$-axis direction and it essentially reproduces 35.07 dBi associated with the reference antenna. The cross-polarized pattern remains low, approximately 55 dB below the main beam. The reference antenna has nominally zero cross-polarized radiation in the principal planes [50]. The H-plane pattern compares similarly with the reference antenna (not shown). The maximum directivity D_0, realized in the $+z$-axis direction, is compared between the two antennas with respect to frequency in Fig. 12(b). The feed pattern is assumed to be nondispersive over the frequency band. The maximum directivity of the reference antenna increases with respect to frequency, as appropriate for a constant-aperture antenna. Due to the resonant nature of meta-atoms, the directivity diminishes away from the design frequency for the metasurface reflector antenna. The 3 dB directivity bandwidth is approximately 36 MHz.

To computationally validate the design effectiveness using full-wave simulation on an available workstation, we have chosen a moderate reflector dimension in this example. The 3641 number of dipoles may be treated using existing DDA

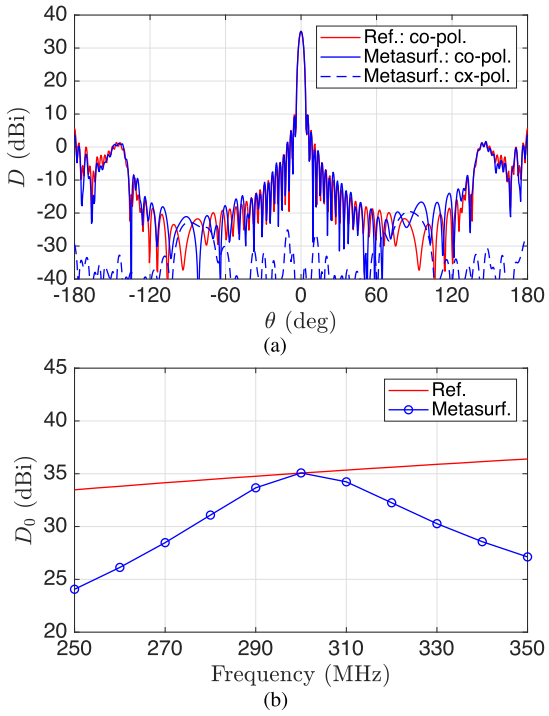

Fig. 12. Directivity pattern characteristics of the parabolic metasurface reflector antenna. (a) Directivity pattern in the E-plane (xz plane) at 300 MHz. The angle θ measures positive toward the $+x$-axis. (b) Maximum directivity in the $+z$-axis direction with respect to frequency.

approaches [33], [35]. Nevertheless, it can be seen that the proposed technique can treat significantly larger metasurfaces, when the number of meta-atoms becomes impractically large to be handled using standard DDA-based techniques.

VII. Conclusion

A design technique for large and infinite metasurfaces of planar and doubly-curved profiles with meta-atoms at nonperiodic, irregular grid points has been presented. The surface is gridded by an unstructured mesher and the meta-atoms are placed at the node locations. Meta-atoms are approximated as point dipoles and the DDA method is employed to evaluate the local E-field that excites each meta-atom. Each meta-atom is individualized using the polarizability that relates the induced dipole moment and the exciting local E-field. Example metasurfaces of planar and paraboloidal profiles for full reflection demonstrate the effectiveness of the design technique. Not based on a periodic meta-atom arrangement, the proposed technique enables nonperiodic metasurfaces of planar and doubly-curved profiles to attain transmission and reflection characteristics approaching those of periodic counterparts based on unit-cell analysis. Application is limited to electrically thin, single-layer, dense metasurfaces that support homogenized tangential electric surface currents.

For planar metasurfaces, irregular grids do not provide visible advantages over periodic designs based on unit-cell analysis. Nevertheless, they provide validation of the design technique before transitioning to doubly-curved surfaces. Main advantages of the design technique lie in synthesizing doubly-curved metasurfaces. An unstructured mesh generator provides a conformal grid with an approximately uniform element spacing. In contrast, regular periodic grids are incompatible with doubly-curved surfaces. Efforts to apply a periodic grid result in cell shape distortions and local meta-atom density changes.

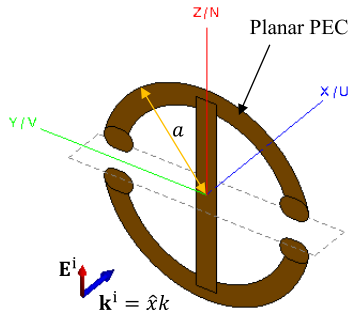

Fig. 13. Plane-wave scattering configuration by an isolated meta-atom in free space using FEKO for polarizability computation.

Future work includes allowing inhomogeneous local transmission and reflection characteristics to realize waveform transformation. An extension to meta-atoms on a grounded dielectric substrate will enable tailoring wave-surface interaction by doubly-curved conformal metasurfaces in the reflective mode. A multilayer array of dipole meta-atoms will be able to independently control reflection and transmission.

Appendix
Numerical Polarizability Extraction

Polarizability in this work is the intrinsic polarizability, that of a single, isolated dipole in free space under a polarizing time-harmonic E-field. In metamaterials and metasurfaces research, the *effective* polarizability [33], [41] is also in use, defined via the induced dipole moment in an infinite array environment relative to the external, illuminating field. For the planar dipole meta-atom in Fig. 4(a), plane-wave scattering simulation configuration in Altair FEKO is shown in Fig. 13. The dipole is tightly contained in a circle of radius a in the yz plane, with the dipole axis along the z-axis. An $+x$-propagating unit plane wave with an E-field $\mathbf{E}^{\mathrm{i}} = \hat{z}e^{-jkx}$ V/m illuminates the dipole.

A z-directed point dipole with an induced dipole moment $\mathbf{p}_z = \hat{z}p_z$ creates a far-zone E-field[3]

$$\mathbf{E} = -\hat{\theta}\frac{k^2 p_z}{4\pi\epsilon_0}\frac{e^{-jkr}}{r}\sin\theta. \tag{16}$$

One form of spherical mode expansion expresses the far-zone dipole E-field as [51]

$$\mathbf{E} = k\sqrt{\eta}Q_{201}^{(4)}\mathbf{F}_{201}^{(4)} = -\hat{\theta}\left(\frac{j}{4}\sqrt{\frac{6\eta}{\pi}}Q_{201}^{(4)}\right)\frac{e^{-jkr}}{r}\sin\theta \tag{17}$$

[3]The dipole axis is set to the z-axis for simpler post processing after FEKO simulation because a z-directed electric dipole field radiates one nonzero spherical mode. An x-directed dipole would produce two nonzero spherical modes.

in the $e^{j\omega t}$ time convention, where $Q_{201}^{(4)}$ is the coefficient for the fundamental electric dipole mode. Equating (16) and (17), the polarizability definition (2) gives

$$\alpha = j\frac{\epsilon_0\sqrt{6\pi\eta}}{k^2}Q_{201}^{(4)}. \tag{18}$$

In a scattering simulation, FEKO natively provides the numerical value of $Q_{201}^{(4)}$. For the dipole meta-atom in Fig. 4(a), FEKO analysis and application of (18) produce the polarizability result in Fig. 4(b).

REFERENCES

[1] C. L. Holloway, E. F. Kuester, J. A. Gordon, J. O'Hara, J. Booth, and D. R. Smith, "An overview of the theory and applications of metasurfaces: The two-dimensional equivalents of metamaterials," *IEEE Antenn. Propag. Mag.*, vol. 54, no. 4, pp. 10–35, Apr. 2012.

[2] S. B. Glybovski, S. A. Tretyakov, P. A. Belov, Y. S. Kivshar, and C. R. Simovski, "Metasurfaces: From microwaves to visible," *Phys. Rep.*, vol. 634, pp. 1–72, Apr. 2016.

[3] H.-T. Chen, A. J. Taylor, and N. Yu, "A review of metasurfaces: Physics and applications," *Rep. Prog. Phys.*, vol. 79, no. 7, Jul. 2016, Art. no. 076401.

[4] J. D. Joannopoulos, S. G. Johnson, J. N. Winn, and R. D. Meade, *Photonic Crystals: Molding Flow Light*, 2nd ed. Princeton, NJ, USA: Princeton Univ. Press, 2008.

[5] F. Yang and Y. Rahmat-Samii, *Electromagnetic Band Gap Structures in Antenna Engineering*. Cambridge, U.K.: Cambridge Univ. Press, 2009.

[6] M. Dupré, L. Hsu, and B. Kanté, "On the design of random metasurface based devices," *Sci. Rep.*, vol. 8, 2018, Art. no. 7162.

[7] H. Nasari, M. Dupré, and B. Kanté, "Efficient design of random metasurfaces," *Opt. Lett.*, vol. 43, no. 23, pp. 5829–5832, Dec. 2018.

[8] S. Savo, N. Papasimakis, and N. I. Zheludev, "Localization of electromagnetic fields in disordered metamaterials," *Phys. Rev. B, Condens. Matter*, vol. 85, no. 12, Mar. 2012, Art. no. 121104(R).

[9] C. Helgert *et al.*, "Effective properties of amorphous metamaterials," *Phys. Rev. B, Condens. Matter*, vol. 79, no. 23, Jun. 2009, Art. no. 233107.

[10] P.-Y. Chen and A. Alu, "Mantle cloaking using thin patterned metasurfaces," *Phys. Rev. B, Condens. Matter*, vol. 84, no. 20, Nov. 2011, Art. no. 205110.

[11] V. Popov, S. N. Burokur, and F. Boust, "Conformal sparse metasurfaces for wavefront manipulation," *Phys. Rev. Appl.*, vol. 14, no. 4, Oct. 2020, Art. no. 044007.

[12] N. M. Estakhri and A. Alù, "Ultra-thin unidirectional carpet cloak and wavefront reconstruction with graded metasurfaces," *IEEE Antennas Wireless Propag. Lett.*, vol. 13, pp. 1775–1778, 2014.

[13] S. M. Kamali, A. Arbabi, E. Arbabi, Y. Horie, and A. Faraon, "Decoupling optical function and geometrical form using conformal flexible dielectric metasurfaces," *Nature Commun.*, vol. 7, no. 1, Sep. 2016, Art. no. 11618.

[14] Y. Shang and Z. Shen, "Polarization-independent backscattering enhancement of cylinders based on conformal gradient metasurfaces," *IEEE Trans. Antennas Propag.*, vol. 65, no. 5, pp. 2386–2396, May 2017.

[15] D. J. Gregoire, "3-D Conformal Metasurfaces," *IEEE Antennas Wireless Propag. Lett.*, vol. 12, pp. 233–236, 2013.

[16] R. C. Rumpf, J. J. Pazos, J. L. Digaum, and S. M. Kuebler, "Spatially variant periodic structures in electromagnetics," *Phil. Trans. Roy. Soc. A, Math., Phys. Eng. Sci.*, vol. 373, no. 2049, Aug. 2015, Art. no. 20140359.

[17] J. Cheng, S. Jafar-Zanjani, and H. Mosallaei, "All-dielectric ultrathin conformal metasurfaces: Lensing and cloaking applications at 532 nm wavelength," *Sci. Rep.*, vol. 6, 2016, Art. no. 38440.

[18] S. Skokic and Z. Sipus, "Moment method analysis of a spherical FSS in free space," in *Proc. 18th Int. Conf. Appl. Electromagn. Commun.*, Oct. 2005, pp. 1–4, doi: 10.1109/ICECOM.2005.205025.

[19] C.-S. Park *et al.*, "Analysis of curved frequency selective surface for radome using characteristic basis function method," in *Proc. 10th Eur. Conf. Antennas Propag. (EuCAP)*, Davos, Switzerland, Apr. 2016, pp. 1–4, doi: 10.1109/EuCAP.2016.7481386.

[20] H. F. Álvarez *et al.*, "3D conformal bandpass millimeter-wave frequency selective surface with improved fields of view," *Sci. Rep.*, vol. 11, 2021, Art. no. 12846.

[21] Z. Sipus, M. Bosiljevac, and S. Skokic, "Analysis of curved frequency selective surfaces," in *Proc. 2nd Eur. Conf. Antennas Propag. (EuCAP)*, Edinburgh, U.K., 2007, p. 145, doi: 10.1049/ic.2007.1268.

[22] Z. Sipus, M. Bosiljevac, and S. Skokic, "Analysis of curved frequency selective surfaces," Univ. Zagreb, Zagreb, Croatia, Tech. Rep. FA8655-07-1-3018, May 2008.

[23] J. Lee and D. F. Sievenpiper, "Method for extracting the effective tensor surface impedance function from nonuniform, anisotropic, conductive patterns," *IEEE Trans. Antennas Propag.*, vol. 67, no. 5, pp. 3171–3177, May 2019.

[24] E. M. Purcell and C. R. Pennypacker, "Scattering and absorption of light by nonspherical dielectric grains," *Astrophys. J.*, vol. 186, pp. 705–714, Dec. 1973.

[25] B. T. Draine and P. J. Flatau, "Discrete-dipole approximation for scattering calculations," *J. Opt. Soc. Amer. A, Opt. Image Sci.*, vol. 11, no. 4, pp. 1491–1499, Apr. 1994.

[26] P. A. Belov and C. R. Simovski, "Homogenization of electromagnetic crystals formed by uniaxial resonant scatterers," *Phys. Rev. E, Stat. Phys. Plasmas Fluids Relat. Interdiscip. Top.*, vol. 72, no. 2, Aug. 2005, Art. no. 026615.

[27] C. R. Simovski and S. A. Tretyakov, "Local constitutive parameters of metamaterials from an effective-medium perspective," *Phys. Rev. B, Condens. Matter*, vol. 75, no. 19, May 2007, Art. no. 195111.

[28] A. D. Scher and E. F. Kuester, "Extracting the bulk effective parameters of a metamaterial via the scattering from a single planar array of particles," *Metamaterials*, vol. 3, no. 1, pp. 44–55, Mar. 2009.

[29] R. A. de la Osa, P. Albella, J. M. Saiz, F. González, and F. Moreno, "Extended discrete dipole approximation and its application to bianisotropic media," *Opt. Exp.*, vol. 18, no. 23, pp. 23865–23871, Nov. 2010.

[30] T. D. Karamanos, A. I. Dimitriadis, and N. V. Kantartzis, "Polarizability matrix extraction of a bianisotropic metamaterial from the scattering parameters of normally incident plane waves," *Adv. Electromagn.*, vol. 1, no. 3, pp. 64–70, Oct. 2012.

[31] P. T. Bowen, T. Driscoll, N. B. Kundtz, and D. R. Smith, "Using a discrete dipole approximation to predict complete scattering of complicated metamaterials," *New J. Phys.*, vol. 14, no. 3, Mar. 2012, Art. no. 033038.

[32] N. Landy and D. R. Smith, "Two-dimensional metamaterial device design in the discrete dipole approximation," *J. Appl. Phys.*, vol. 116, no. 4, Jul. 2014, Art. no. 044906.

[33] L. Pulido-Mancera, P. T. Bowen, M. F. Imani, N. Kundtz, and D. Smith, "Polarizability extraction of complementary metamaterial elements in waveguides for aperture modeling," *Phys. Rev. B, Condens. Matter*, vol. 96, no. 23, Dec. 2017, Art. no. 235402.

[34] L. Pulido-Mancera, M. F. Imani, P. T. Bowen, N. Kundtz, and D. R. Smith, "Analytical modeling of a two-dimensional waveguide-fed metasurface," 2018, *arXiv:1807.11592*.

[35] I. Yoo, M. F. Imani, L. Pulido-Mancera, T. Sleasman, and D. R. Smith, "Analytic model of a coax-fed planar cavity-backed metasurface antenna for pattern synthesis," *IEEE Trans. Antennas Propag.*, vol. 67, no. 9, pp. 5853–5866, Sep. 2019.

[36] L. M. Pulido-Mancera, T. Zvolensky, M. F. Imani, P. T. Bowen, M. Valayil, and D. R. Smith, "Discrete dipole approximation applied to highly directive slotted waveguide antennas," *IEEE Antennas Wireless Propag. Lett.*, vol. 15, pp. 1823–1826, 2016.

[37] L. M. Pulido-Mancera, M. F. Imani, and D. R. Smith, "Discrete dipole approximation for the simulation of the edge effects on metasurfaces," in *Proc. IEEE Int. Symp. Antennas Propag. (APSURSI)*, Fajardo, PR, USA, Jun. 2016, pp. 107–108.

[38] R. Zecca, D. L. Marks, and D. R. Smith, "Variational design method for dipole-based volumetric artificial media," *Opt. Exp.*, vol. 27, no. 5, pp. 6512–6527, Mar. 2019.

[39] D. Pande, J. Gollub, R. Zecca, D. L. Marks, and D. R. Smith, "Symphotic multiplexing medium at microwave frequencies," *Phys. Rev. Appl.*, vol. 13, no. 2, Feb. 2020, Art. no. 024033.

[40] R. E. Collin, *Field Theory of Guided Waves*. New York, NY, USA: McGraw-Hill, 1960, ch. 12.

[41] S. Tretyakov, *Analytical Modeling in Applied Electromagnetics*. Norwood, MA, USA: Artech House, 2003.

[42] P.-O. Persson and G. Strang, "A simple mesh generator in MATLAB," *SIAM Rev.*, vol. 46, no. 2, pp. 329–345, 2004.
[43] H. Edelsbrunner, *Analytical Modeling in Applied Electromagnetics*. Cambridge, U.K.: Cambridge Univ. Press, 2001.
[44] W. L. Stutzman and G. A. Thiele, *Antenna Theory Design*, 3rd ed. Hoboken, NJ, USA: Wiley, 2013.
[45] S. I. Maslovski and S. A. Tretyakov, "Full-wave interaction field in two-dimensional arrays of dipole scatterers," *Int. J. Electron. Commun. (AEÜ)*, vol. 53, no. 3, pp. 135–139, 1999.
[46] J. D. Jackson, *Classical Electrodynamics*, 3rd ed. Hoboken, NJ, USA: Wiley, 1999.
[47] X. Ni, Z. J. Wong, M. Mrejen, Y. Wang, and X. Zhang, "An ultrathin invisibility skin cloak for visible light," *Science*, vol. 349, no. 6254, pp. 1310–1314, Sep. 2015.
[48] P. Gurrala, S. Oren, P. Liu, J. Song, and L. Dong, "Fully conformal square-patch frequency-selective surface toward wearable electromagnetic shielding," *IEEE Antennas Wireless Propag. Lett.*, vol. 16, pp. 2602–2605, 2017.
[49] A. Chatterjee and S. K. Parui, "Frequency-dependent directive radiation of monopole-dielectric resonator antenna using a conformal frequency selective surface," *IEEE Trans. Antennas Propag.*, vol. 65, no. 5, pp. 2233–2239, May 2017.
[50] C. A. Balanis, *Antenna Theory: Analysis and Design*, 4th ed. Hoboken, NJ, USA: Wiley, 2016.
[51] J. E. Hansen, Ed., *Spherical Near-Field Antenna Measurements*. Stevenage, U.K.: The Institution of Engineering and Technology, 1988.

Do-Hoon Kwon (Senior Member, IEEE) received the B.S. degree from the Korea Advanced Institute of Science and Technology (KAIST), Daejeon, South Korea, in 1994, and the M.S. and Ph.D. degrees from The Ohio State University, Columbus, OH, USA, in 1995 and 2000, respectively, all in electrical engineering.

He was a Senior Engineer with Samsung Electronics, Suwon, South Korea, from 2000 to 2006. From 2006 to 2008, he was a Post-Doctoral Researcher with the Material Research Science and Engineering Center and the Department of Electrical Engineering, Pennsylvania State University, University Park, PA, USA. In 2008, he joined the Department of Electrical and Computer Engineering, University of Massachusetts Amherst, Amherst, MA, USA, where he is currently affiliated with the Antennas and Propagation Laboratory. He spent the summer of 2011 as a Summer Faculty Fellow with the Sensors Directorate of the Air Force Research Laboratory, Wright-Patterson Air Force Base, OH, USA. In 2014, he has published a coedited book *Transformation Electromagnetics and Metamaterials: Fundamental Principles and Applications* (Springer). From 2016 to 2017, he was a Visiting Professor with the Department of Electronics and Nanoengineering, Aalto University, Espoo, Finland. His main research interests include the bandwidth properties of antennas and arrays, small/wideband antennas, frequency-selective surfaces, microwave metamaterials and metasurfaces, cloaking, and transformation electromagnetic/optical device designs.

Dr. Kwon received the inaugural IEEE Antennas and Propagation Society Edward E. Altshuler Prize Paper Award in 2011.